Review Paper

Experimental Conditions for Improved Confinement Modes in Heliotron J

MIZUUCHI Tohru, SANO Fumimichi, KONDO Katsumi[1)], NAGASAKI Kazunobu, OKADA Hiroyuki, KOBAYASHI Shinji, YAMAMOTO Satoshi[*], TORII Yuki, HANATANI Kiyoshi, NAKAMURA Yuji[1)], SUZUKI Yasuhiro[1)♣], KANEKO Masashi[1)], ARIMOTO Hajime[1)], ARAKAWA Jun[1)], AZUMA Takahisa[1)], HAMAGAMI Takashi[1)], KIKUTAKE Masaaki[1)], MOTOJIMA Gen[1)], OHASHI Keisuke[1)], SHIMAZAKI Nobuhide[1)], YAMADA Masaki[1)], YAMAZAKI Hisamichi[1)], KITAGAWA Hiroki[1)], NAKAMURA Hidenori[1)], TSUJI Takayuki[1)], WATANABE Shinya[1)], IJIRI Yoshiyuki, SENJU Tohru, YAGUCHI Keiji, SAKAMOTO Kinzo, TOSHI Kiyoshi and SHIBANO Masashi

Institute of Advanced Energy, Kyoto University, Gokasho, Uji 611-0011, Japan.

[1)] Graduate School of Energy Science, Kyoto University, Gokasho, Uji 611-0011, Japan.

(Received 5 April 2005 / Accepted 22 September 2005)

ECH/NBI experiments in Heliotron J have revealed the existence of a spontaneous transition to improved confinement modes. Based on the experimental database obtained up to now, the characteristics of the transition and the density and power thresholds are discussed paying attention to the configuration effects. For ECH+NBI discharges with injection powers of P_{ECH} ~ 0.29 MW and P_{NBI} ~ 0.57 MW, transition phenomena were observed in almost all $\iota(a)/2\pi$ configurations. The global plasma confinements before and after the transition are affected by the value of the edge rotational transform $\iota(a)/2\pi$. During the improved mode, the $\iota(a)/2\pi$-dependence of the plasma stored energy is mitigated compared to the pre-transition phase. The database indicates the existence of a critical value in the line-averaged electron density under which the transition cannot be observed. This threshold line-averaged density is in the range of $1.1–2.0\times10^{19}$ m^{-3} in most configurations, indicating that it is not a strong function of the injection power and/or the heating method. The existence of an $\iota(a)/2\pi$ value where the transition was not observed for ECH-only discharges but observed for NBI-only or ECH+NBI discharges suggests the existence of a configuration effect and/or heating-method effect on the threshold power.

Keywords:

improved plasma confinement, H-mode, Heliotron J, helical-axis heliotron, configuration effect, density threshold

1. Introduction

The Heliotron J device [1-3] is a flexible concept-exploration facility for optimization of the helical-axis heliotron configuration [4]. This configuration is one of the advanced helical configurations based on the quasi-isodynamic approach. The advanced helical concept is frequently characterized by the Fourier components of the confinement field in the Boozer coordinates. In the helical-axis heliotron concept, in addition to toroidicity and helicity, bumpiness is introduced as a third knob to control the neo-classical transport. As for the MHD stability in high-β plasmas, the Heliotron J device creates a magnetic well for the whole confinement region instead of the strong edge magnetic shear in conventional heliotrons.

One of the main objectives of the Heliotron J experiment is to study configuration effects on the plasma performance: the effects of each Fourier component of the confinement field, effects of the existence of rational surfaces, effects of the magnetic shear and/or magnetic well, effects of the distance to the first wall or other plasma facing materials, etc. This configuration study should be performed not only from the neoclassical transport viewpoint but also from the anomalous transport viewpoint. Although the helical-axis heliotron concept aims at the reduction of neoclassical transport, the control of anomalous transport is one of the key issues in plasma experiments. The formation of internal transport barriers (ITB) and/or edge transport barriers (ETB), which is

author's e-mail: mizuuchi@iae.kyoto-u.ac.jp

This article is based on the invited talk at the 21th JSPF Annual Meeting (Shizuoka, 2004).

[*] *Present affiliation: Graduate School of Engineering, Osaka University, Suita, Japan*

[♣] *Present affiliation: National Institute for Fusion Science, Toki, Japan*

observed in many tokamaks and some stellarators, is also an attractive phenomenon for the helical-axis heliotron concept.

The Heliotron J experiments have revealed the existence of "good" confinement states compared to the energy confinement time scaling in stellarators, the ISS95 scaling [5]. For higher-density discharges under these "good conditions", we have found a spontaneous transition to improved confinement modes [6]. Here the increase in the stored energy and core electron density is observed after the spontaneous drop of the intensity of $H\alpha/D\alpha$-emission. These observations are similar to the characteristics of the H-mode in tokamaks. There are some reports of these kinds of observations in Heliotron J for ECH-only [7-9], NBI-only and ECH+NBI plasmas [10,11]. Recently, the configuration effects on the transition were studied by changing the edge rotational transform $\iota(a)/2\pi$ as a label of the configuration [12].

This paper reviews these experimental observations of the transition to improved modes in Heliotron J and discusses the conditions for the transition.

2. Experiments

The details of the Heliotron J device are described in Ref. [3]. The coil system of the device consists of a continuous helical field coil (HFC) with high pitch-modulation, two sets of toroidal field coils (TFC-A and TFC-B, 8-coils/set) and three pairs of vertical field coils: the main vertical field coil (MVFC), the inner vertical field coil (IVFC) and the auxiliary vertical field coil (AVFC). Due to the strong pitch modulation of the $M = 4$ helical coil, the toroidal shape of the plasma looks square in the top view as shown in Fig. 1. Due to the introduction of bumpiness in the field component, the strength of the confinement field on the magnetic axis is higher at the "corner sections" than that at the "straight sections" in regular configurations. Figures 2 (a) and (b) show the shape of the magnetic surfaces and the mod-B contours at the corner and straight sections, respectively. After the initial experimental verification of the sound magnetic surfaces [3], the initial plasma experiments were performed by using 53 GHz ECH systems in FY2000-2001 [13,14]. After these experiments, the installation of other heating systems was performed: a 70 GHz ECH system [15] ($P_{ECH} \leq 0.4$ MW) in FY2001, and one beam-line of a tangential NBI system (30 keV, 0.7 MW, H^0-beam) and an ICRF system with a loop antenna (~ 20 MHz, 0.5 MW) in FY2003 [16].

The first 70 GHz-ECH experiment was performed using the second-harmonic ECH with a well-focused Gaussian beam (the beam radius at the magnetic axis is about 2 cm) [15], where the microwaves were launched from a horizontal port located at one of the corner sections of Heliotron J (see Fig. 1) [7, 8]. The first experimental findings of a spontaneous transition to an improved confinement mode in Heliotron J were obtained with this ECH system. After that, the launching position of the 70 GHz microwave beam was moved from the horizontal port at the "corner section" to a top port at one of the "straight sections" of the device (see Fig. 1). Due to the mechanical limitation in this section, the focusing and steer-

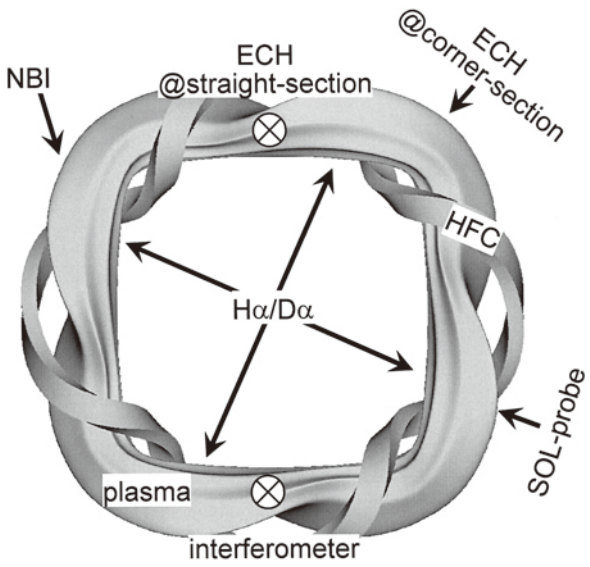

Fig. 1 A schematic view of the Heliotron J device.

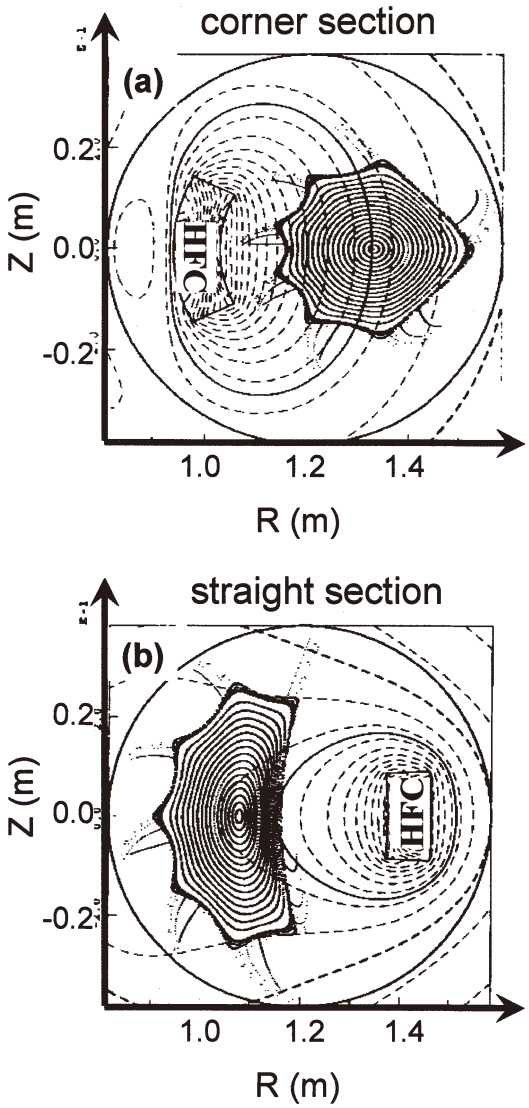

Fig. 2 Shape of the magnetic surfaces and the mod-B contour for the standard configuration at (a) the corner section and (b) straight section.

ing system of the launcher, which was used in the horizontal launching experiments, was not installed, and a non-focused Gaussian beam was launched. Here, the beam radius at the magnetic axis is about 6 cm. Since the mod-B structure and the beam focusing are different for each launching position, a significant difference is expected in the power deposition profile and the total power absorption rate for these launching conditions. The single-path power deposition profile and the |B|-dependence of the total single-path power absorption rate for each launching condition were evaluated using the ray-tracing code TRECE [17]. Figures 3 (a) and (b) show typical examples of the calculations (assuming T_e = 0.5 keV and $\bar{n}_e$ = 1×10^{19} m^{-3}) for horizontal well-focused launching and vertical (non-focused) launching, respectively. In the latter case, due to the non-focusing launching, the deposition profile is much wider than that in the former case. On the other hand, the total single-path power absorption rate is limited to ~ 60 % in the horizontal launching case due to the steep gradient of the magnetic field strength at the corner section while that for the vertical launching case is ~ 100 %.

For NBI-only or ECH+NBI plasmas, the target plasma was produced by the second-harmonic 70 GHz ECH. Although the working gas for the target ECH plasmas has been changed from hydrogen to deuterium since the FY2004 campaign for ICRF H^+-minority heating experiments, the H^0-beam has been injected in the NBI heating case.

In order to research the transition condition under a fixed configuration and a heating scheme with a fixed value of input power, the line-averaged electron density was controlled by changing pre-programmed gas puffing from 2–4 valves distributed around the torus.

For the first-step configuration study in Heliotron J, we focused on the change in the global confinement property for different values of the edge rotational transform ι(a)/2π. The Heliotron J device can produce a wide variety of field configurations by changing the combination of the coil currents. It is not so easy, however, to control only ι(a)/2π while keeping constant all other geometrical parameters (the magnetic axis position, the plasma volume, the distance from the plasma facing materials, etc.) and combinations of Fourier components of the confinement field (helicity, toroidicity, bumpiness, etc.). Therefore, it should be considered that ι(a)/2π is a label of the configuration. Up to now, we have tried to change ι(a)/2π in two ways: by controlling the poloidal fields [6] and by controlling the current ratio of HFC and TFCs [12]. In the latter case, coil currents were selected to maintain both the magnetic axis position and the field strength on the axis at the ECH launching section in order to realize the central plasma heating condition.

The important diagnostics are diamagnetic loops for W_p^{dia}, an interferometer for $\bar{n}_e$, and $H\alpha/D\alpha$ detectors (see Fig. 1). Changes in edge plasma properties were monitored with a poloidal array of Langmuir probes located in the SOL (SOL probe). The array has four probe pins (each 5 mm apart). The first pin with a fixed bias voltage was used for the ion-saturation current (I_s) measurement, the second and third pins were

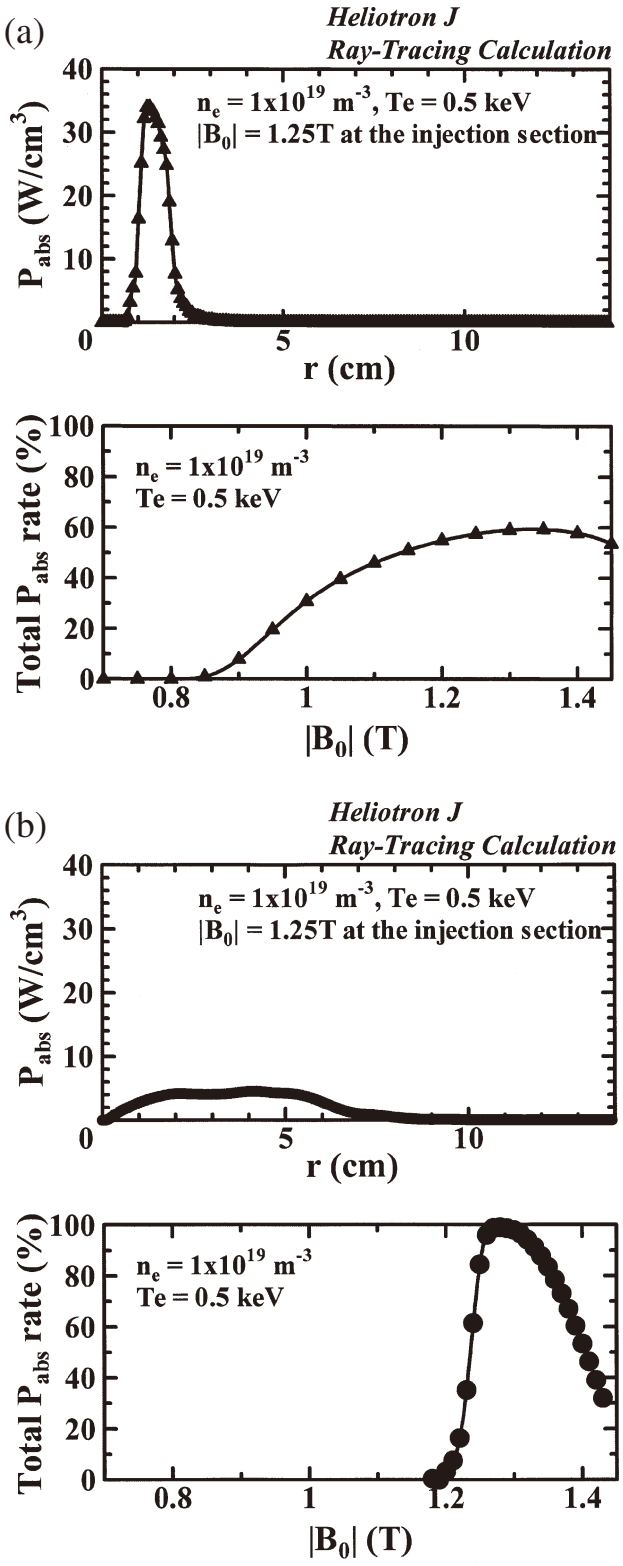

Fig. 3 Single path power deposition profile and total power absorption rate for (a) the horizontal well-focused launching and (b) the vertical (non-focusing) launching cases.

used for the floating potentials (V_f) at two different poloidal positions, and the fourth pin was used with 100-Hz scanning bias voltage for the estimation of electron temperature (T_e). These probe pins are aligned nearly parallel to the shape of

the calculated last closed flux surface (LCFS) in the poloidal cross section of the torus. The radial position of the probe R-R_{LCFS} can be changed on a shot-by-shot basis. Here R is the radial position of the probe along the major radius and R_{LCFS} is the radial position of the last closed flux surface under the vacuum condition.

3. Characteristics of the Spontaneous Transition to the Improved Confinement

3.1 ECH-only plasmas

The first experimental findings of a spontaneous transition to an improved confinement mode in Heliotron J were obtained in second-harmonic on-axis ECH experiments with a well-focused Gaussian beam (70 GHz, 0.3 MW) from the horizontal port. Figure 4 shows an example of the time history of ECH discharge (H^+ plasma in this case) in the configuration of $\iota(a)/2\pi \approx 0.542$. Spontaneous drops in the $H\alpha$ signal and ion-saturation current of the SOL probe located near the last closed flux surface I_s, and a subsequent rise in the line-averaged density $\bar{n}_e$ and in the plasma stored energy measured with diamagnetic loops W_p^{dia} were observed. The increment in the plasma energy $\Delta W_p^{dia}/W_p^{dia}$ reached ~ 70 %. The estimated global energy confinement time τ_E^{exp} was 1.7 times longer than that expected from the ISS95 scaling τ_E^{ISS95}, whereas τ_E^{exp} just before the transition was almost at the scaling level. Since it was difficult to control the density increase after the transition, it was not sure that the observed τ_E^{exp} was the maximum one obtainable under the heating condition in this field configuration.

After the change of the launching position of the microwaves, similar transition phenomena were observed again for second-harmonic ECH plasmas [11].

The transition could be observed only for higher-density discharges for both launching cases. The threshold density, below which the H-mode transition is not obtained, is almost the same value for both launching conditions. The details are discussed in Sec. **4**.

3.2 NBI-only plasmas

A similar spontaneous transition to an improved confinement mode was also observed for NBI (H^0 beam of ~ 28 keV) plasmas [10,11]. Figure 5 shows an example of the time history of NBI-only discharge in the standard configuration ($\iota(a)/2\pi \approx 0.560$). After a few ms from the end of the 70 GHz ECH short pulse, the co-injection of NB (the port through power was P_{NBI} ~ 0.5 MW) was turned on to the afterglow plasma for this shot. During the NBI pulse, the gas-puff was kept on to increase the density. As shown in the figure, two clear drops in $H\alpha/D\alpha$ intensity were observed in this discharge. The first one starts at t ~ 207 ms and ends at ~ 222 ms. The second one starts at a higher density timing (t ~ 255 ms). In some cases, more than two transitions were observed during a single shot. Although the change in the increasing rate of $\bar{n}_e$ is not clear in this particular shot, W_p^{dia} starts to increase when intensities of $H\alpha/D\alpha$ and I_s drops. The increases of $\bar{n}_e$ and W_p^{dia} are stopped when the $H\alpha/D\alpha$ intensity and I_s return to a higher level.

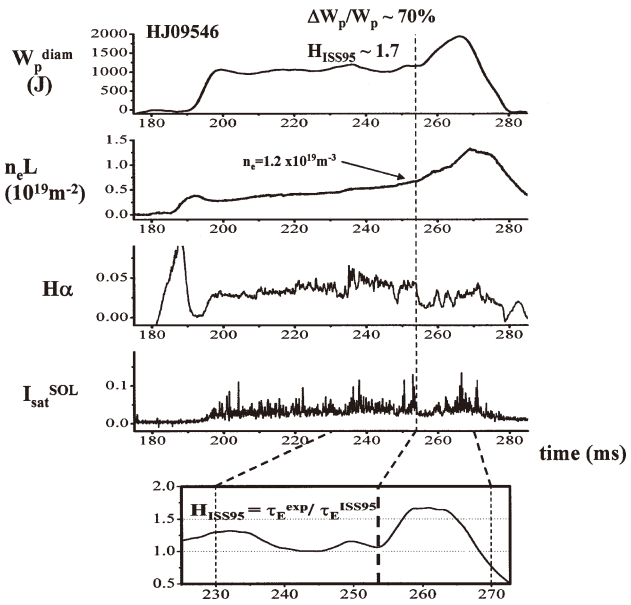

Fig. 4 Time history of an ECH-only discharge in the configuration of $\iota(a)/2\pi \approx 0.542$ with the transition to the improved mode [8].

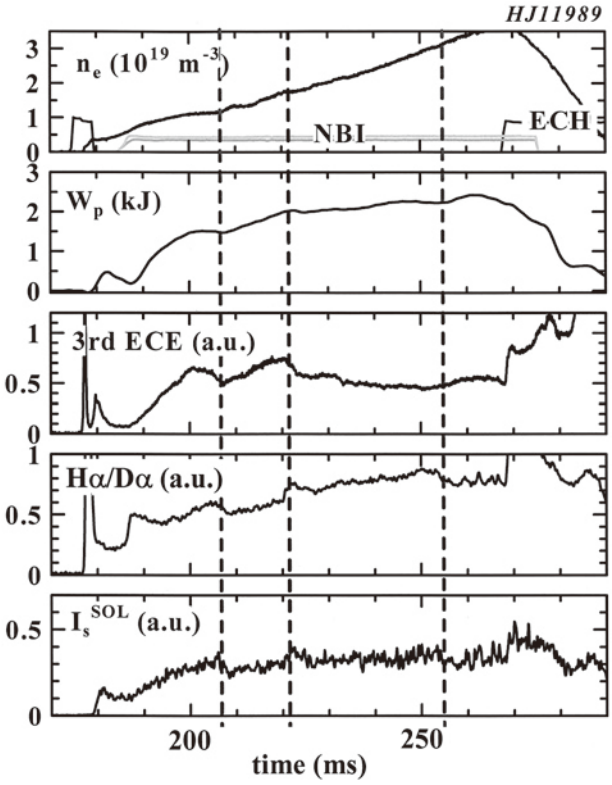

Fig. 5 Time history of an NBI-only discharge in the standard configuration ($\iota(a)/2\pi \approx 0.560$) with the transition to the improved mode [11].

It is interesting to note that the above-mentioned characteristics of the transition were clearly observed for the first transition event. As typically shown in Fig. 5, 10–15 ms after from the NBI is turned on, the third-harmonic ECE signal I_{ECE} and W_p^{dia} stop increasing or start to decreasing, which

indicates the occurrence of confinement degradation. After that, the transition to the improved mode seems to come about if $\bar{n}_e$ is high enough near this timing. The lower limit of $\bar{n}_e$ for the transition is ~ 1.1–1.5×10^{19} m^{-3}, and it does not depend on P_{NBI} in the range of 0.3–0.55 MW.

During the low-$H\alpha/D\alpha$ phase, it was observed that the increasing rate of SX photo-diode array signals was larger than that at other timings [11]. This tendency is clear for the edge chord. After the back transition, the increasing rate of the signal for edge chords decreases whereas that for the center chords does not change. This indicates that the SX-signal profile become more peaked after the back transition. These observations suggest that the change of confinement occurs in the edge region.

3.3 ECH+NBI plasmas

Figure 6 shows an example of the time history of ECH+NBI combination heating discharge for the standard configuration (ι(a)/2π ≈ 0.560) [11]. The initial plasma was produced and heated by 70 GHz microwaves (second-harmonic ECH, P_{ECH} ~ 0.3 MW). After ~ 15 ms from the start of ECH, the NBI (P_{NBI} ~ 0.5–0.6 MW) was superposed up to the end of the ECH pulse. Due to a rather low gas-puffing rate in the earlier phase of this discharge and to the density clamping caused by ECH, the NB was injected to a rather low-density target plasma. Increasing the gas-puffing rate, the density increased gradually beyond the cut-off density of the second-harmonic X-mode. A clear drop in the $H\alpha/D\alpha$ signal was observed at t ~ 242 ms and the signal intensity was kept at a low level up to the end of the discharge. At almost the same time, the increasing rate of W_p^{dia} was enhanced. Depending on the density evolution, some "dithering" of $H\alpha/D\alpha$ intensity and/or ion-saturation currents in the edge region was observed before the transition (This phase is similar to that defined as Phase I in [12]). During the dithering phase, neither W_p^{dia} nor $\bar{n}_e$ decreases.

Besides these H-mode like transitions, the ι(a)/2π scan in the FY2004 campaign revealed the existence of two different types of transition to improved modes at two different ι(a)/2π values, ~ 0.50 and 0.61. They have different characteristics in their pre-transition phase from the H-mode-like transition described above. Figures 7 and 8 show examples of time traces of such discharges at ι(a)/2π ~ 0.51 and 0.61, respectively.

The spontaneous transition observed at ι(a)/2π ~ 0.51 is characterized by the appearance of low-frequency and large-amplitude oscillations in the signals of W_p^{dia}, $\bar{n}_e$, I_p and $H\alpha/D\alpha$ before the spontaneous increase of W_p^{dia} and $\bar{n}_e$ (Fig. 7). As shown in the figure, W_p^{dia} and $\bar{n}_e$ (and $H\alpha/D\alpha$ intensity) are almost constant before the appearance of the oscillation. The non-inductive plasma current (mainly the bootstrap current and the beam-induced current) is gradually increasing in this phase. Before and during the oscillation phase, no clear MHD-activity is observed as shown in the figure. Since the value of ι(a)/2π is close to a low mode resonance condition, the islands near the rational surface might be related with this low-frequency oscillation. For example, the non-inductive plasma current can change in ι(a)/2π and cause large-scale

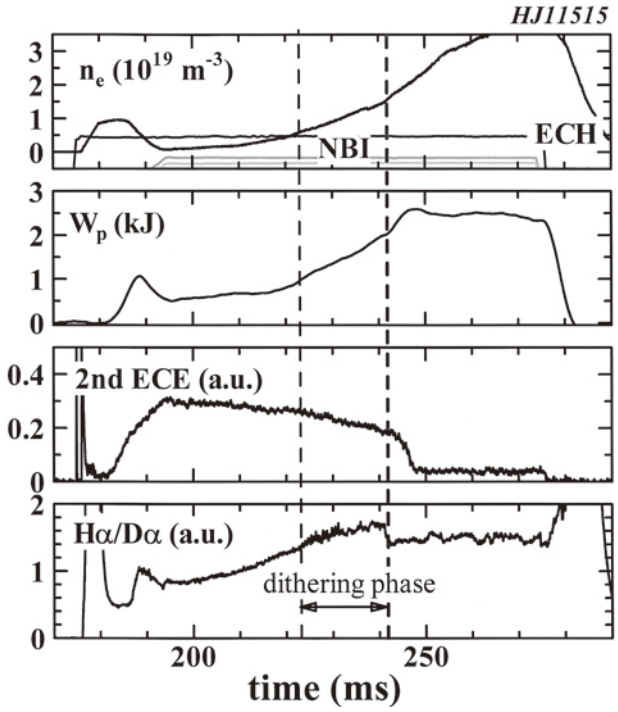

Fig. 6 Time history of an ECH+NBI discharge in the standard configuration (ι(a)/2π ≈ 0.560) with the transition to the improved mode [11].

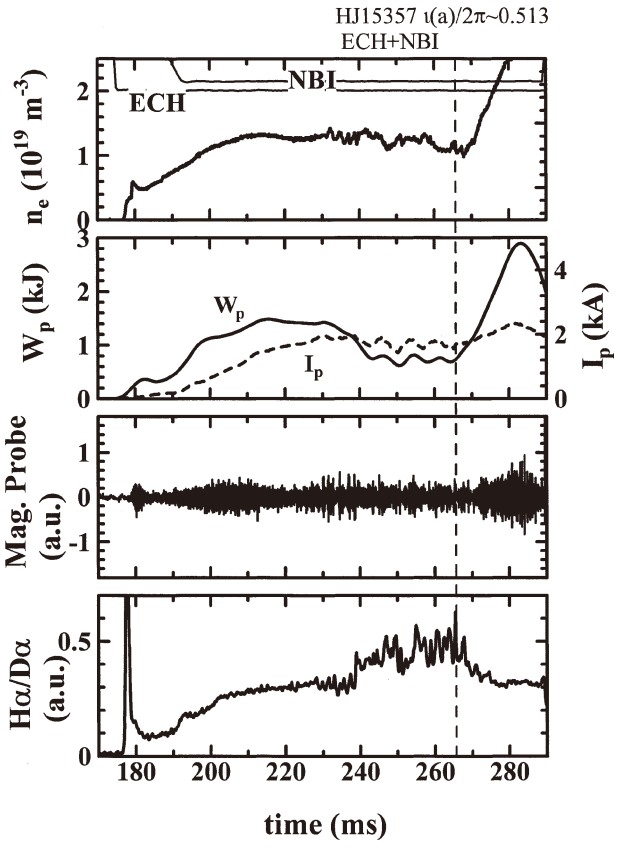

Fig. 7 Time history of an ECH+NBI discharge in the configuration of ι(a)/2π ≈ 0.513.

deformation of the flux surfaces and/or resultant contact with the wall. At a certain timing (~ 267 ms for the discharge shown in Fig. 7), the oscillation is spontaneously stopped and W_p^{dia} and $\bar{n}_e$ start to rapidly increase beyond the level before the oscillation. In this W_p^{dia}-increase phase, $H\alpha/D\alpha$ intensity decreases to a lower level almost the same as that observed before the oscillations, although $\bar{n}_e$ increases far beyond that before the oscillation phase.

Another different type of transition observed at $\iota(a)/2\pi \approx 0.611$ is characterized by the occurrence of strongly bursting MHD modes before the spontaneous increase of W_p^{dia} and $\bar{n}_e$ (see Mag. probe in Fig. 8) [18]. According to the analysis of the magnetic probe signals, the toroidal mode number of the MHD modes should be ≈ 3. These bursting modes seem to degrade the confinement: W_p^{dia} and $\bar{n}_e$ are decreased or suppressed after the appearance of bursting MHD modes. A decrease of ECE signals is simultaneously observed. At a certain timing (~ 263 ms for the discharge shown in Fig. 8), however, the confinement is spontaneously improved, and the values of W_p^{dia} and $\bar{n}_e$ are rapidly increased although similar-type of MHD activities are still observed.

Although these two types of spontaneous change of the confinement state are very interesting and important phenomena, our present database on these events is not yet sufficient to understand the mechanisms of these unfavorable behaviors of plasma and the physical processes of the transitions to favorable states.

3.4 Edge plasma properties

Figure 9 shows an example of the time evolutions of W_p^{dia} and $\bar{n}_e$, and $H\alpha/D\alpha$ signals at two different toroidal positions (see Fig. 1), the radiation loss measured with an AXUV diode, and I_s at R-R_{LCFS} = 2.7 cm for an ECH+NBI plasma at $\iota(a)/2\pi \approx 0.54$. The fluctuation-induced particle flux $\tilde{\Gamma}_{fluct}$ is also plotted in the figure, which is estimated from the equation $\tilde{\Gamma}_{fluct} \propto \tilde{I}_s \times (\tilde{V}_f^1 - \tilde{V}_f^2)$, where $\tilde{I}_s$ is the fluctuation component of the ion-saturation current and $\tilde{V}_f^1$, $\tilde{V}_f^2$ are the floating potential fluctuations from two different pins for the V_f measurement [19]. The positive value of $\tilde{\Gamma}_{fluct}$ corresponds to the outward flow. At the timing of a rapid $H\alpha/D\alpha$ drop (~ 248 ms), the value of I_s suddenly decreases; the normalized fluctuation level, $\tilde{I}_s/\bar{I}_s$, and $\tilde{\Gamma}_{fluct}$ decrease simultaneously. In this particular shot, repetitive increases and decreases in $\tilde{\Gamma}_{fluct}$ were observed during the time interval of 218 ms < t < 248 ms in correspondence with the dithering of the $H\alpha/D\alpha$ signal. Sharp spikes with large amplitudes were also observed in I_s, V_f (not shown in the figure) and $\tilde{\Gamma}_{fluct}$, indicating the intermittent nature of the edge plasma turbulence. After the transition, the intensity of such intermittent bursts decreased. Since the averaged values of $\tilde{\Gamma}_{fluct}$ also decreased after the transition, it is not clear at present whether the apparent decrease of burst level indicates a change in the characteristics of the turbulence.

Figure 10 shows the radial distributions of I_s, V_f, T_e and $\tilde{\Gamma}_{fluct}$ before and after the transition obtained by changing the probe position on a shot-by-shot basis. Due to the poor time resolution of the T_e measurement with the SOL probe, the

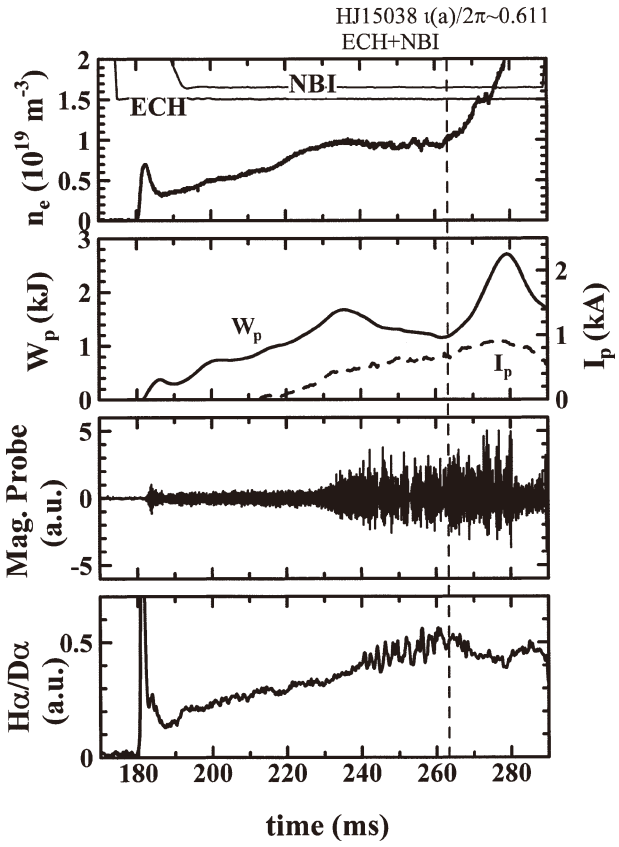

Fig. 8 Time history of an ECH+NBI discharge in the configuration of $\iota(a)/2\pi \approx 0.611$.

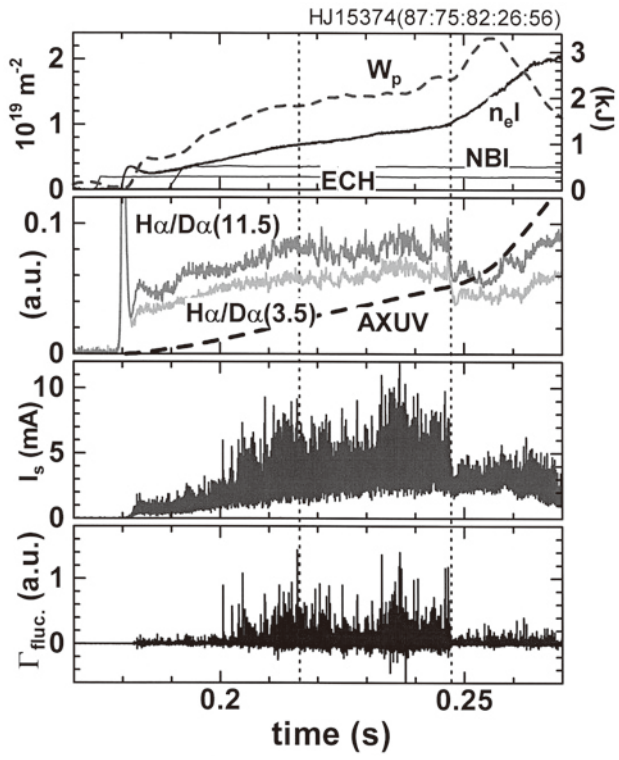

Fig. 9 Time history of an ECH+NBI discharge in the configuration of $\iota(a)/2\pi \approx 0.538$. The SOL probe position is R-R_{LCFS} = 2.7 cm.

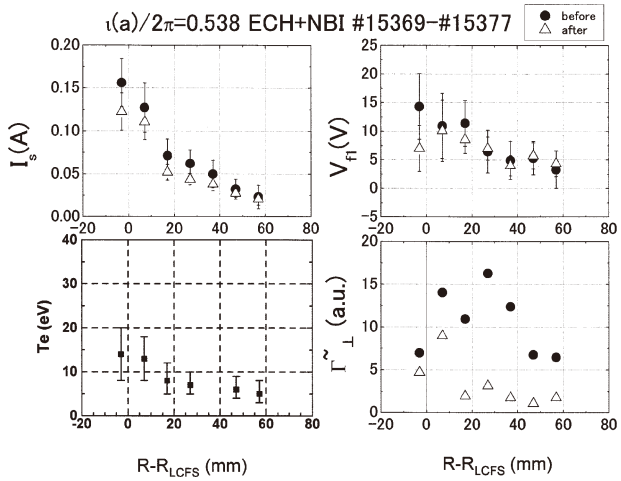

Fig. 10 Radial profiles of the ion-saturation current, floating potential, electron temperature, and fluctuation-induced particle radial flux from the SOL probe before and after the transition for the same discharge series as the shot shown in Fig. 9.

averaged T_e near the transition timing is plotted in this figure. The radial profile of I_s is a monotonically decreasing function of R-R_{LCFS} for both timings before and after the transition. The change in the radial profile of I_s around the transition timing is not clear for this particular discharge set. This suggests that the transport barrier might be set at an inner region from LCFS beyond the available radial range of the movable probe. On the other hand, a change in the V_f-profile is observed. The profile of the floating potential after the transition has a positive maximum near R-R_{LCFS} = 1.0 cm whereas the floating potential monotonically increases with insertion of the probe toward and beyond the last closed flux surface before the transition (~ 248 ms). In order to study the effect of the radial electric field E_r on the plasma turbulence and resultant particle flux, the space potential (V_p) profile should be investigated instead of the V_f-profile. Neglecting the change of T_e through the transition, the drop of V_f near the last closed flux surface suggests the change of the radial electric field from positive to negative (or a significant change of the E_r-shear) after the transition.

As will be discussed in next section, the transition to the improved confinement mode is observed in all configurations investigated so far. A clear change of the radial electric field such as shown in Fig. 10 was observed only for some limited field configurations and/or heating scenarios. It is interesting to note that such a clear change of V_f-profile, indicating the formation of negative E_r, was observed only for the transitions with higher improvement factors as defined in the next section [20]. The detailed investigation of the relation between the formation of the negative E_r (or E_r-shear) and the transition to the improved mode and/or its impact on the edge plasma turbulence remains as a future work including the confirmation of the edge transport barrier.

4. Discussion

4.1 Effects of the magnetic field configuration

The investigation of configuration effect on the transition phenomena, especially the effects of the edge rotational transform, is one of the key issues in the Heliotron J program since the operating condition of the H-mode in W7-AS is strongly related to the rotational transform [21]. It is not so easy to scan only ι(a)/2π without changing other configuration parameters as mentioned in Sec. **2**. Moreover, non-inductive plasma currents (bootstrap currents, beam induced currents and/or ECCD currents) can change the edge rotational transform. Although the absolute values of such non-inductive currents are not so large, they can change the topology of the edge field lines, especially near the resonance condition. Nevertheless, as the first step of the investigation, we take the edge rotational transform ι(a)/2π in a vacuum condition.

In Refs 6 and 9, we reported the existence of two operational ι(a)/2π-windows for the transition; $0.54 < \iota(a)/2\pi < 0.56$ (a magnetic limiter configuration) and $0.62 < \iota(a)/2\pi < 0.63$ (a partially wall-limiter configuration), where the configuration was controlled by changing the vertical field. In the FY2004 campaign, more detailed investigations of the configuration effects on the occurrence of the transition were performed for the ι(a)/2π-range of 0.49–0.64 [12]. Here, the ι(a)/2π was changed by controlling the ratio of the field strength by HFC and that by TFCs, keeping the magnetic axis position nearly constant in order to maintain the central plasma heating of ECH as well as NBI. These studies revealed that transition phenomena were observed for almost all ι(a)/2π configurations investigated in the FY2004 campaign, at least for the input power range in these experiments. The only one exception was the case of ECH-only discharges for the configuration of $\iota(a)/2\pi \approx 0.493$, where no transition was observed for the available ECH power range. For NBI-only or ECH+NBI discharges, however, the transition was observed in the same configuration.

In order to discuss the quality of the improved mode, in Ref. 12, we take the ISS95 scaling as a measure of confinement. Here, it is observed that the ι(a)/2π-values for good confinement, where the peak values of $\tau_E^{exp}/\tau_E^{ISS95}$ are over 1.3, are slightly less than the values for major natural resonances. In such ι(a)/2π-conditions, the enhancement factor of $\tau_E^{exp}/\tau_E^{ISS95} \approx 1.8$ is observed. When ι(a)/2π is far from the "good" values, the enhancement of $\tau_E^{exp}/\tau_E^{ISS95}$ is only minor.

On the other hand, in order to discuss the improvement by the transition itself, it is worth looking at the improvement factor defined as the ratio of the maximum W_p^{dia} during the improved mode to that just before the transition. As shown in Fig. 11, the experiment has also revealed that the improvement factor also depends on the configuration. Some configurations show a remarkable improvement factor (> 2) whereas the improvement factor for other configurations stays at 1.2–2. It is interesting to note that W_p^{dia} increases by a factor of 2 or more even when the enhancement of $\tau_E^{exp}/\tau_E^{ISS95}$ is minor.

Near the resonance condition of ι(a)/2π, the edge mag-

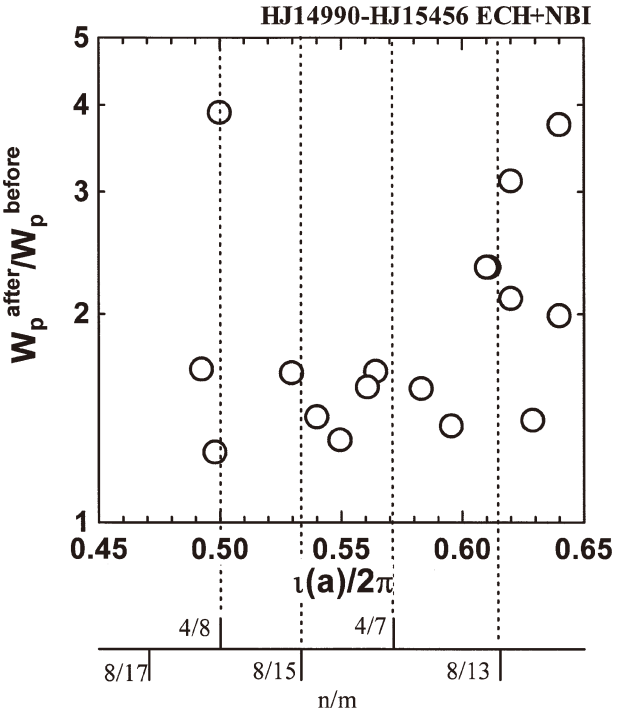

Fig. 11 Configuration effect on the ratio of the maximum W_p^{dia} during the improved mode to that at just before the transition. (ECH+NBI discharges with P_{ECH} ~ 0.29 MW and P_{NBI} ~ 0.57 MW).

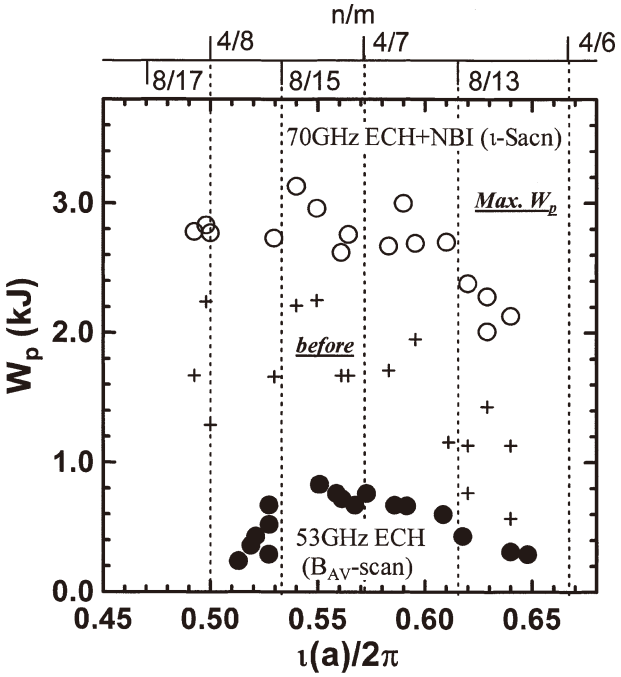

Fig. 12 Maximum W_p^{dia} obtained during the improved mode as a function of ι(a)/2π (the same discharge set as the for Fig. 11). The data from Ref. [14] are also plotted as a reference.

netic surfaces are strongly modified by the edge natural island chain, or the size of the last closed flux surface is reduced in a low magnetic shear device as observed in W-7AS [22,23]. This effect results in the fine structure of ι(a)/2π-dependence (i.e. clear degradation of the confinement near the major resonance condition of ι(a)/2π) in W-7AS. The first configuration experiment in Heliotron J from this point of view was performed using the 53 GHz ECH (oblique injections with non-focusing TE_{02}-mode, P_{in} ~ 0.4 MW) and initial observations on the effect of ι(a)/2π on the plasma performance were reported in Refs. 13 and 14. Here the ι(a)/2π was changed through the control of the vertical field (Fig. 3 in Ref. 14), and the maximum attainable value of W_p^{dia} was surveyed by carefully tuning the gas-puffing rate for each ι(a)/2π configuration. In this 53 GHz ECH experiment, we observed the fine structure of ι(a)/2π-dependence, but it was not so clear compared to the result in W-7AS. In addition, this experiment also revealed that the obtainable value of W_p^{dia} under the same input power had a global tendency to decrease as ι(a)/2π departed from ι(a)/2π ≈ 0.54.

Figure 12 shows the ι(a)/2π dependence of the maximum W_p^{dia} during the improved mode (○) for the ι(a)/2π-scan experiment (ECH+NBI discharges with a fixed input power) in the FY2004 campaign [12]. The figure includes data from the configurations of ι(a)/2π ~ 0.51 and 0.61, where degradation of the plasma confinement is observed in the pre-transition phase. In this figure, the data reported in Ref. 14 are also plotted as a function of ι(a)/2π for reference. Regarding the global ι(a)/2π-dependence, it is found that higher W_p^{dia} is obtained again near ι(a)/2π ≈ 0.54 also for the improved mode, and that W_p^{dia} decreases for ι(a)/2π away from this value. It is interesting to compare the global tendency between the 53 GHz and 70 GHz ECH cases using normalized values (i.e. $W_p^{dia}/W_p^{diamax.}$) for each case. The global ι(a)/2π dependence become mild in the improved mode, especially for ι(a)/2π < 0.52. As discussed in Refs. 13 and 14, the plasma-wall interaction is considered a potential explanation for the global tendency. Since ι(a)/2π was controlled by different ways in these two experiments and the distances between the LCFS and the wall were not the same, we should make more careful investigation to understand the observed difference in the global tendency between the two conditions.

Relating to the improvement factor discussed with Fig. 11, it is interesting to focus on the fine structure in ι(a)/2π dependence before and after the transition. In Fig. 12, the values of W_p^{dia} just before the transition are plotted by (+). For the data from the pre-transition phase, a clear fine structure in the dependence of W_p^{dia} on ι(a)/2π is observed. In the pre-transition phase, W_p^{dia} is clearly low near the major resonance condition of ι(a)/2π. During the improved phase, however, such a fine structure becomes not so clear, resulting in a high improvement factor for some ι(a)/2π configurations as shown in Fig. 11. This suggests that the transition to the improved mode mitigates the sensitive dependence of W_p^{dia} on ι(a)/2π.

4.2 Density threshold for the transition

The transition to the improved mode has been observed only for discharges with densities higher than a certain value. According to Ref. 12, the threshold is in the range of $\bar{n}_e$ ~ 1.1–1.3×10^{19} m^{-3} for the 70 GHz second harmonic ECH dis-

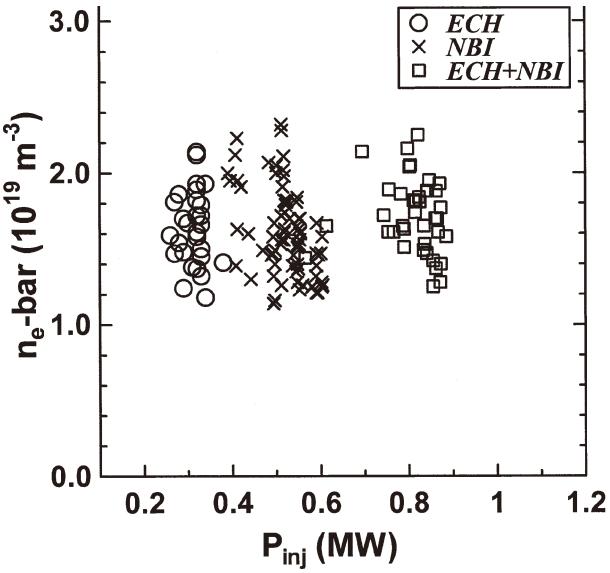

Fig. 13 Relation of the density and the injection power at the incidence of the transition for different heating schemes in the standard configuration [25].

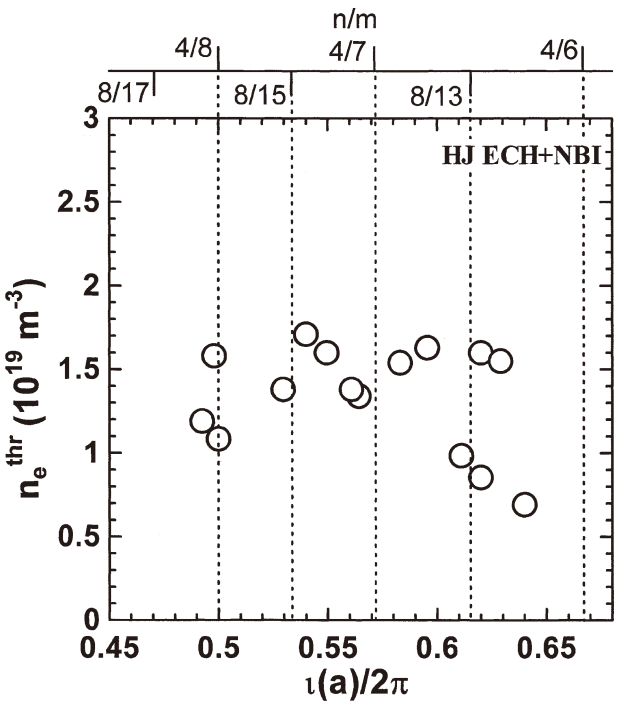

Fig. 14 Lower density limit to obtain the transition for several $\iota(a)/2\pi$ values (ECH+NBI discharges with P_{ECH} ~ 0.29 MW and P_{NBI} ~ 0.57).

charges in the standard configuration ($\iota(a)/2\pi \approx 0.560$). Figure 13 shows the relation of the density and the injection power at the incidence of the transition in the standard configuration for ECH-only, NBI-only and ECH+NBI plasmas [25]. The absence of data points in the low-density region ($\bar{n}_e \leq 1\times10^{19}$ m^{-3}) means that the transition could be observed only for the higher-density region. The threshold density (lower density limit for the transition) is again in the range of $\bar{n}_e \sim 1.1\times10^{19}$ m^{-3}. Moreover, this graph indicates that this threshold value is not sensitive to the heating method and injection power level.

In the FY2004 campaign, the density thresholds for the different configurations were investigated for ECH+NBI discharges with P_{ECH} ~ 0.29 MW and P_{NBI} ~ 0.57 MW. Figure 14 shows the threshold density required to obtain the transition for several $\iota(a)/2\pi$ values. The figure suggests that the threshold density is in the range of 1.1–2.0×10^{19} m^{-3} in most cases. In the previous section, the fine structure of $\iota(a)/2\pi$-dependence for W_p^{dia} was discussed. Checking Fig. 14 from this point of view, a fine structure in $\iota(a)/2\pi$-dependence is found similar to the dependence of W_p^{dia} in the pre-transition phase. Near the major resonance condition of $\iota(a)/2\pi$, the threshold density is low. This similarity could be partially understood by the strong dependence of W_p^{dia} on the density. For higher values of $\iota(a)/2\pi$ (> 0.6), however, the figure shows the existence of some exceptional low-threshold density cases (lower than ~ 1×10^{19} m^{-3}). In these configurations, the density in the pre-transition phase stayed a low level and was difficult to increase by gas puffing. Although the confinement degradation is concerned also for these configurations like the $\iota(a)/2\pi \approx 0.61$ case discussed in the previous section, there were no clear signals suggesting MHD activities and/or oscillations for these cases. It is remained as a future work to investigate the confinement degradation mechanism for these discharges and the physical process by which the improved mode.

The threshold density at the standard configuration ($\iota(a)/2\pi \approx 0.560$) is about 1.3×10^{19} m^{-3} in this experiment. This threshold density seems to be slightly higher than that for the previous experiments. Although the FY2004 campaign was performed with D^+ target plasmas, it is not clear at present whether the isotope effect makes such difference or not. More detailed experiments should be necessary with taking care of the wall conditioning.

As for the density threshold, it should be noted that both the H-to-L and L-to-H transitions are observed in the density range higher than the threshold value as shown in Fig. 5. This fact suggests that the line-averaged density is not a sufficient condition for the transition but a necessary condition.

4.3 Effects of total heating power

H-mode studies in tokamaks indicate that another necessary condition for the transition is the heating power or the power outgoing through LCFS. Based on the tokamak database, some empirical formulas for the required power for the L-to-H transition are introduced as a function of the line-averaged density, the surface area of LCFS, the strength of the confinement field, etc. [26].

Figure 15 shows the threshold density for several absorption power levels (0.1 MW < P_{abs} < 0.5 MW) at $\iota(a)/2\pi$ ~ 0.498 (one of the high $\tau_E^{exp}/\tau_E^{ISS95}$ configurations). Here the P_{ECH} was controlled for ECH-only discharges and P_{NBI} was changed for ECH+NBI discharges under a fixed value of P_{ECH}. Although the number of data points is not large enough so far, there is no clear or simple relation between the threshold density and the absorption power. In Fig. 15,

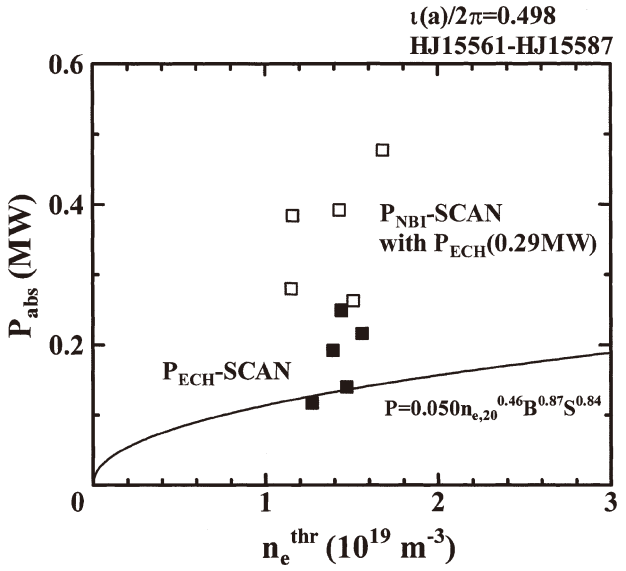

Fig. 15 Threshold density for several absorption power levels (0.1 MW < P_{abs} < 0.5 MW) of ECH-only and ECH+NBI discharges in the configuration of $\iota(a)/2\pi \approx 0.498$. The solid curve in the figure denotes the threshold power estimated by using a scaling formula for the H-mode in tokamaks [26].

the solid curve denotes the threshold power for the H-mode transition in tokamaks, which is simply calculated using the scaling formula reported in Ref. 26. As shown in the figure, the minimum power level examined in the experiment, i.e. the operation limit of our power source of microwaves, is almost the same level as the threshold power expected from the tokamak scaling. Similar results are obtained for another configuration of $\iota(a)/2\pi \sim 0.56$ (the standard configuration). No clear power dependence on the threshold density shown in Fig. 15 is consistent with the result shown in Fig. 13, where the differences in the density threshold are not significant among the various heating schemes and power levels under fixed field configuration.

It is interesting to note that for ECH-only discharges at $\iota(a)/2\pi \approx 0.493$, the transition was not obtained for the available ECH power range. For ECH+NBI discharges, however, the transition was observed. This suggests the existence of some configuration effects and/or heating-method effect on the power threshold.

4.4 Effects of heating profile

According to the ECH experiments in Heliotron J with a well-focused microwave beam [27], both the on- and off-axis heating conditions can produce plasmas of a wide density region $\bar{n}_e < 2\times10^{19}$ m^{-3}, where the upper density range is probably limited by the cut-off of the second harmonic X-mode in the central region. However, optimal heating (i.e. higher W_p^{dia}) was found only for the condition of highly localized on-axis heating (r/a < 1/4). The experimental energy confinement time, τ_E^{exp}, could increase the ratio $\tau_E^{exp}/\tau_E^{ISS95}$ above unity (up to ~ 1.5-2) for this optimal heating condition, but the off-axis heating could not reach such a high level of $\tau_E^{exp}/\tau_E^{ISS95}$. In those experiments, only high-density discharges in the on-axis heating were accompanied by the spontaneous transition to the improved confinement mode. This observation raises the question of whether the heat deposition affects the occurrence of the transition. In tokamak H-mode studies, preferable effects of the edge ECH heating on the L-to-H transition have been reported [28]. The experiments under the two different ECH launching conditions in Heliotron J might give us a hint on the effect of the power deposition profile on the occurrence of the transition.

As shown in Fig. 3, the single-path power deposition profile is quite different between these two launching conditions. The peak absorption-power-density in the well-focused case is about 6-7 times higher than that in the non-focusing case. However, we observed the transition for both cases at least for the input power level of $P_{ECH} \sim 0.3$ MW. This suggests that the power absorption profile itself is not a primary factor for the transition whenever the on-axis heating condition is maintained. However, it should be noted that the total single-path absorption rate for the horizontal launching case was ~ 60 %, whereas that for the vertical launching case was ~ 100 %. When we take into account the power absorption of the reflected power, the effective power absorption profile could become wider than that shown in Fig. 3(a) for the horizontal launching case. Therefore, the actual difference in the absorption profile between the two cases would diminish. Experiments using off-axis heating would be necessary to clear up this question.

5. Summary

The Heliotron J experiments have revealed the existence of a spontaneous transition to improved confinement modes for all tested heating scenarios (ECH-only, NBI-only and ECH+NBI heating). Based on the experimental database obtained up to now, characteristics of and conditions for the transition are discussed, focusing on the configuration effects.

For the ECH+NBI discharges with the input power of $P_{ECH} \sim 0.29$ MW and $P_{NBI} \sim 0.57$ MW, the effect of the field configuration on the occurrence of the transition was studied by controlling $\iota(a)/2\pi$ as a label of the configuration. Our findings are as follows:

(1) the transition phenomena is observed for almost all $\iota(a)/2\pi$ configurations under this range of input power,
(2) the $\iota(a)/2\pi$-ranges for good confinement, where the peak values of $\tau_E^{exp}/\tau_E^{ISS95}$ reach 1.3–1.8 during the improved mode, are located in the regions slightly below the major natural resonances,
(3) in the pre-transition phase, W_p^{dia} is conspicuously low near the major resonance condition of $\iota(a)/2\pi$,
(4) the drop of W_p^{dia} is moderated after the transition.

The transition is observed only for discharges with a density higher than a critical value. As for this density threshold, we can summarize as follows:

(1) the threshold line-averaged density for the transition is in the range of 1.1–2.0×10^{19} m^{-3} in most cases,
(2) near the major resonance condition of $\iota(a)/2\pi$, the threshold density becomes low,
(3) in the higher $\iota(a)/2\pi$-region ($\iota(a)/2\pi > 0.6$), some exceptional low-density cases exist,
(4) the line-averaged density is not a sufficient condition for the transition but a necessary condition.

As for the threshold of the input power,
(1) there is no clear or simple relation between the threshold density and the absorption power for a fixed field configuration,
(2) here, the minimum power level examined so far, i.e. the operation limit of our power source of microwaves, is almost the same level as the threshold power expected from the tokamak scaling. However,
(3) the existence of a configuration for which the transition was not observed only with ECH discharges suggests the existence of some configuration effect and/or heating-method effect on the threshold power.

We need to continue theoretical and experimental investigations to understand the observed transition phenomena and to attain long pulse operation with high-quality, improved confinement state in Heliotron J.

Acknowledgments

The work was partially supported by the Collaboration Program of the Laboratory for Complex Energy Processes, IAE, Kyoto University, the Kyoto University 21st century COE Program and the National Institute of Fusion Science (NIFS) Collaborative Research Program.

References

[1] T. Obiki *et al.*, Nucl. Fusion **39**, 1667 (1999).
[2] F. Sano *et al.*, J. Plasma Fusion Res. SERIES, Vol.**3**, 26 (2000).
[3] T. Obiki *et al.*, Nucl. Fusion **41**, 833 (2001).
[4] M. Wakatani *et al.*, Nucl. Fusion **40**, 569 (2000).
[5] U. Stroth *et al.*, Nucl. Fusion **36**, 1063 (1996).
[6] F. Sano *et al.*, Fusion Sci. Technol. **46**, 288 (2004).
[7] F. Sano *et al.*, *30th EPS Conference on Contr. Fusion and Plasma Phys.*, St. Petersburg, 7-11 July 2003 ECA Vol.27A, O-2.2A.
[8] F. Sano *et al.*, J. Plasma Fusion Res. **79**, 1111 (2003).
[9] F. Sano *et al.*, *14th Int. Stellarator Workshop* (Greifswald, Sept., 2003), I.Tu.1., http://www.ipp.mpg.de/eng/for/veranstaltungen/workshops/stellarator_2003/index.html.
[10] T. Mizuuchi *et al.*, *14th Intern. Stellarator Workshop* (Greifswald, Sept. 2003), O.Tu 3.
[11] T. Mizuuchi *et al.*, Plasma Sci. Technol. **6**, 2371 (2004).
[12] F. Sano *et al.*, *20th IAEA Fusion Energy Conference* (Vilamoura, Portugal, Nov. 2004), IAEA-CN-116/EX/9-2.; *in print* Nucl. Fusion.
[13] T. Obiki *et al.*, J. Plasma Fusion Res. SERIES **5**, 288 (2002).
[14] T. Obiki *et al.*, *13th Int. Stellarator Workshop* (Feb. 2002, Canberra) OI-9, http://wwwrsphysse.anu.edu.au/admin/stellarator/proceedings.html.
[15] H. Shidara *et al.*, J. Plasma Fusion Res. SERIES **5**, 333 (2002).
[16] S. Kobayashi *et al.*, *20th IAEA Fusion Energy Conference*, (Vilamoura, Portugal, Nov. 2004), IAEA-CN-116/EX/P4-41.
[17] H. Shidara *et al.*, J. Plasma Fusion Res. **81**, 48 (2005).
[18] S. Yamamoto *et al.*, in Workshop on "Improvement of MHD Stability through Control of Magnetic Structure and Plasma Pressure Profile in Toroidal Plasmas", (Feb. 2005, Toki).
[19] T. Mizuuchi *et al.*, J. Nucl. Mater. **337-339**, 332 (2005).
[20] K. Ohashi, Master Theses (March 2005), Graduate School of Energy Science, Kyoto University (in Japanese).
[21] F. Wagner *et al.*, *19th IAEA Fusion Energy Conference* (Lyon, 2002) OV2-4.
[22] R. Jaenicke *et al.*, Nucl. Fusion **33**, 687 (1993).
[23] R. Brakel, Plasma Phys. Control. Fusion **39**, B273 (1997).
[24] H. Okada *et al.*, J. Plasma Fusion Res. **80**, 883 (2004).
[25] Y. Fukagawa, Master Theses (March 2004) Graduate School of Energy Science, Kyoto University (in Japanese).
[26] for example, J.A. Snipes *et al.*, *19th IAEA Fusion Energy Conference* (Lyon, 2002) CT/P-40.
[27] T. Obiki *et al.*, Nucl. Fusion **44**, 47 (2004).
[28] K. Hoshino *et al.*, Nucl. Fusion **28**, 301 (1988).